RAA 2020 Vol. **20** No. **11**, 185(9pp) doi: 10.1088/1674-4527/20/11/185

http://www.raa-journal.org *http://iopscience.iop.org/raa*

***R**esearch in*
***A**stronomy and*
***A**strophysics*

Has LIGO detected primordial black hole dark matter?

- tidal disruption in binary black hole formation

Yuan Gao[1], Xiao-Jia Zhang[2] and Meng Su[3]

[1] Department of Physics, The University of Hong Kong, Hong Kong SAR, China; *u3502132@hku.hk*
[2] Department of Earth Sciences, The University of Hong Kong, Hong Kong SAR, China; *xzhang17@hku.hk*
[3] Department of Physics and Laboratory for Space Research, The University of Hong Kong, Hong Kong SAR, China; *mengsu84@hku.hk*

Received 2020 March 9; accepted 2020 May 3

Abstract The frequent detection of binary mergers of $\sim 30\,M_\odot$ black holes (BHs) by the Laser Interferometer Gravitational-Wave Observatory (LIGO) rekindled researchers' interest in primordial BHs (PBHs) being dark matter (DM). In this work, we investigated PBHs distributed as DM with a monochromatic mass of $30\,M_\odot$ and examined the encounter-capture scenario of binary formation, where the densest central region of DM halo dominates. Thus, we paid special attention to the tidal effect by the supermassive black hole (SMBH) present. In doing so, we discovered a necessary tool called loss zone that complements the usage of loss cone. We found that the tidal effect is not prominent in affecting binary formation, which also turned out to be insufficient in explaining the totality of LIGO's event rate estimation, especially due to a microlensing event constraining the DM fraction in PBH at the mass of interest from near unity to an order smaller. Meanwhile, an early-universe binary formation scenario proves so prevailing that the LIGO signal in turn constrains the PBH fraction below one percent. Thus, people should put more faith in alternative PBH windows and other DM candidates.

Key words: black hole physics — dark matter — gravitational waves — quasars: supermassive black holes

1 INTRODUCTION

The advent of gravitational wave (GW) astronomy has opened a new gate into probing the universe. Since the first confirmed binary black hole (BH) merger event in 2015, there have been nine more detections of the same type and one of binary neutron stars (NSs) (Abbott et al. 2016b,a, 2017; Abbott et al. 2017a,b, 2019). All binary BH events feature component mass on the order of ~ 10 solar masses ($M_\odot$) or beyond, and seven reach the order of $30\,M_\odot$ or above.

On one hand, such masses are generally too heavy for stellar BHs that form from dying stars, whose mass is usually on the order of $\sim 1\,M_\odot$. A more likely candidate might be primordial BHs (PBHs) that formed from gravitationally collapsed over-densities in the radiation dominated era. The formation of PBHs is not related to stellar gravitational collapse, and is majorly attributed to an increased cosmological energy density, thus their masses could span a much wider range (Carr et al. 2016).

On the other hand, their frequent detection suggests a relatively abundant underlying population, which reminds people of the possibility that PBHs might constitute dark matter (DM). DM is a hypothetical model motivated by observations such as the flattening of galaxy rotation curves (see, for example, Corbelli & Salucci 2000) that implies the existence of a considerable amount of unknown masses throughout the galactic region. It is now believed to comprise $\sim$ 85% of all matter content in the universe. As PBHs formed in the radiation-dominated era, they are essentially non-baryonic and qualify for constituting DM (Carr et al. 2016), an idea that arose since the earliest studies of PBHs (Chapline 1975). Also, despite various observational constraints on the fraction of DM in PBHs across their wide range of masses, $30\,M_\odot$ has not been ruled out for PBHs to constitute a major part of DM (Clesse & García-Bellido 2015; Bird et al. 2016). Non-detection in 30 years of searches for an alternative DM candidate called weakly interacting massive particles (WIMPs) such as a supersymmetry particle or the axion

(Jungman et al. 1996; Preskill et al. 1983) also encouraged the study of PBHs' candidature.

Thus it is intriguing to ask if the Laser Interferometer Gravitational-Wave Observatory (LIGO) has detected PBH DM, and whether its GW detection could shed light on the the mass, fraction, etc. of PBHs in constituting DM. Specifically, we would like to know whether PBHs distributed as DM would form binary mergers with an event rate compatible with LIGO's estimation of $9.7 - 101\ \mathrm{Gpc}^{-3}\,\mathrm{yr}^{-1}$ (Abbott et al. 2019). To do so, we first decided on the appropriate population distribution of the proposed PBH DM, then looked at the condition of binary PBH formation. As a starting point, we focused on PBHs with a monochromatic mass function of $\sim 30\,M_\odot$ in a Milky Way (MW)-like galaxy. Throughout this study, we worked under the unit system with $G = c = 1$.

To find out the PBH DM distribution, we noted that N-body simulations of the dark halo have indicated the formation of a dense core at the center distributed as a power law with index ~ -1, though a precise parametric profile has not been resolved between several candidates such as the Navarro-Frenk-White (NFW) and Einasto profiles (Merritt et al. 2006). However, this only takes into account the particle DM component without involving stars and the supermassive black hole (SMBH) at the galactic center. Where they are present, the density slope in the central region is believed to be further steepened to a power of ~ -2 (O'Leary et al. 2009) due to segregation of the PBHs, yet should vanish at the capture radius of the SMBH (Gondolo & Silk 1999), resulting in a 'spike' density profile. Thus we considered all mentioned effects, and adopted the most appropriate distribution within their validity ranges.

PBHs can form binaries via two-body and three-body encounters. Quinlan & Shapiro (1989) and Lee (1993) have demonstrated that binary formation via three-body encounter is only non-negligible in small halos and generically leads to wide binaries that will not merge within the Hubble time. Thus in this work we focused on the two-body scenario where two PBHs emit enough GW energy during a close encounter and capture each other. In such case, the galactic center where DM is the densest shall dominate the binary encounter, and we calculate the capture rate considering current best knowledge of the dark halo distribution. We also take into account the SMBH's tidal effect, which is most prominent at the galactic center as well. Then by convolving the rate calculation in a single MW-like halo with the halo mass function, the merger rate density per comoving volume can be compared with LIGO's estimation of $9.7 \sim 101\ \mathrm{Gpc}^{-3}\,\mathrm{yr}^{-1}$. This might support or constrain the PBH DM proposal.

The rest of this paper is arranged as follows. We review the available density distributions that combine the properties of both DM and PBH, and decide on the most appropriate one for this work in Section 2. Then we look at binary capture mechanism in Section 3, and find the effective binary formation rate in Section 4 taking into account the tidal disruption effect. We present and discuss the results in Section 5, and draw a conclusion in Section 6.

2 DARK MATTER DISTRIBUTION IN THE PRIMORDIAL BLACK HOLE PERSPECTIVE

The NFW profile is a widely accepted and applied DM halo density distribution, obtained by N-body simulation of resolved DM particles evolving from some initial density perturbation spectrum (Navarro et al. 1997). The mass density distribution is described as

$$\frac{\rho(\boldsymbol{r})}{\rho_{\rm crit}} = \frac{\delta_c}{r_*(1+r_*)^2}\,, \tag{1}$$

where $\rho_{\rm crit}$ is the critical density of the universe, and r_* is the galactocentric distance normalized by a scale radius R_s which relates to the virial radius by a concentration parameter $c = \frac{R_{\rm vir}}{R_s}$ that is dependent on the halo mass.

This is not accurate, however, as it only takes account of the DM particles without considering the baryonic component of the galaxy. It becomes most important especially near the galactic center, where an SMBH is generally believed to reside, which steepens the potential well. Here we compare two models that take care of such effect: mass segregation and DM spike. However, these studies are based on the MW, and we start by examining the case of our own Galaxy first.

The effect of mass segregation states that, according to simulation, for a mixed population with lighter but dominant stars and heavier but non-dominant stellar objects - for which PBHs qualify, the existence of the SMBH would result in the heavier population segregating into the center, forming a cusp with power index ~ -2 (O'Leary et al. 2009). Although baryonic dominance in the inner galaxy has not been universally validated, studies have provided some confirmation for disk galaxies, summarized in Courteau & Dutton (2015). Here as we first look at the inner region of the MW, baryonic dominance is highly probable and the mass segregation model is applicable. Moreover, we also found the result in agreement with the spike model to be introduced later, which adds to our confidence. According to O'Leary et al. (2009), various studies have agreed that $\sim$20 000 $10\,M_\odot$ BHs should have segregated into the inner 1 pc of a MW like galaxy, by which we normalize the mass distribution of the segregated profile.

$$\rho_{\rm seg} = \frac{7.7\times10^{-10}}{r^2} m^{-2}\,. \tag{2}$$

The drawback of this model is that it does not go deep into the galactic center where the density starts to drop

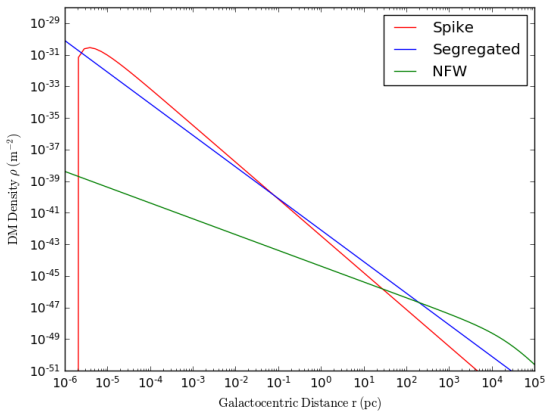

Fig. 1 DM density distributions.

and vanishes by the capture radius of the SMBH $r_{\rm cap} = 4R_\bullet$, four times its Schwarzschild radius (Merritt et al. 2011). Within this distance, objects are believed to directly plunge into the SMBH. Thus we considered a second approach, which studied the effect of an SMBH on the particle DM distribution like NFW, and also agrees with a ~ -2 cusp but does vanish properly (Gondolo & Silk 1999). The profile is called a 'spike' to distinguish it from the segregated cusp. This study, however, does not consider the gravitational effect due to the stellar component, and is restricted to the region of $\leq 0.2\,$pc where the SMBH dominates the gravitational potential. Thus we could treat this as a more accurate description of the PBH DM distribution at the innermost galactic center. From an initial distribution of $\rho(r)_i = \rho_0(r/r_0)^{-\gamma}$, $0 < \gamma < 2$, the spike density profile is given by

$$\rho(r)_{\rm sp} = \rho_0 \left(\frac{R_{\rm sp}}{r_0}\right)^{-\gamma} \left(1 - \frac{r_{\rm cap}}{r}\right)^3 \left(\frac{R_{\rm sp}}{r}\right)^{\gamma_{\rm sp}}, \quad (3)$$

where $\gamma_{\rm sp} = \frac{9-2\gamma}{4-\gamma}$, $R_{\rm sp} = \alpha_\gamma r_0 \left(\frac{M_\bullet}{\rho_0 r_0^3}\right)^{\frac{1}{3-\gamma}}$ and $M_\bullet$ is the mass of the SMBH. α_γ is numerically derived for different values of γ, where for an NFW initial profile with $\gamma = 1$, it was taken to be 0.122. Concretely, in the case of the MW

$$\rho(r)_{\rm sp} = \frac{1.04\times10^{-4}}{r^{\frac{7}{3}}} \left(1 - \frac{5.04\times10^{10}}{r}\right)^3 m^{-2}. \quad (4)$$

The three profiles (NFW, segregated and spike) for a MW-like galaxy are plotted in Figure 1 for comparison.

It turned out that different profiles are applicable to their validity ranges. The spike profile is most accurate within $\sim 0.2\,$pc where the SMBH dominates stellar dynamics, and it transitions to the segregated profile where stellar objects play a large part, and is finally replaced by the NFW profile at $\sim 200\,$pc where DM starts to dominate the population and its N-body simulation becomes more accurate. In the following calculation of binary capture rate, we will utilize this composite of density distributions.

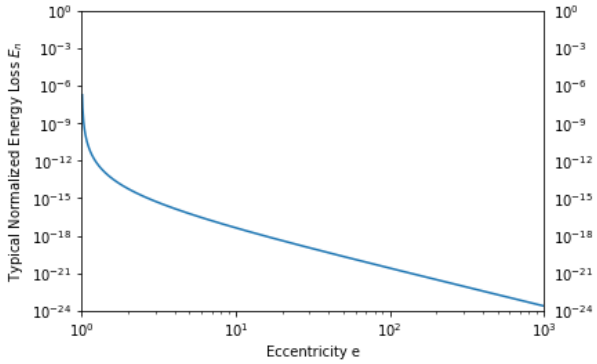

Fig. 2 Normalized energy loss with typical relative velocity $\sim 150\ {\rm km\,s^{-1}}$ at equal-mass binary setup, over orbital eccentricity.

3 CAPTURE OF BINARY BLACK HOLES

A BH binary can form if ample energy is lost via GW radiation during a close encounter. The situation is specified by four parameters, m_1, m_2, $\boldsymbol{r_r}$ and $\boldsymbol{w}$, namely the masses, relative position and relative velocity.

The first step is to consider the energy loss along a complete Keplerian hyperbolic orbit, assuming two BHs approaching each other from infinity. As energy radiation along the path drives the binary closer than the unperturbed orbit, more energy will be actually lost. Thus this approximation provides a conservative maximum impact parameter b for capture. In this case, the magnitude of the relative velocity w and impact parameter b will take the place of the two vector parameters. Turner (1977) calculated the energy loss for an arbitrary unbound orbit at the Newtonian limit, which is the most reliable result used today. Though the non-relativistic approximation is obvious, an analytic solution taking care of the strong gravitational field near periapsis has not yet been obtained. We will stick to Turner's result here.

Setting $G = c = 1$, the radiation is given in Turner (1977) by

$$\delta E = \frac{8}{15} M\eta^2 w^7 f(e)\,, \quad (5)$$

where M is the total mass of the binary, η is the symmetric mass ratio $\frac{m_1 m_2}{M^2}$, e is the orbital eccentricity expressed as $\sqrt{1 + \frac{b^2 w^4}{M^2}}$ and $f(e)$ is an enhancement factor defined by

$$f(e) = \frac{24\cos^{-1}(\frac{1}{e})(1 + \frac{73}{24}e^2 + \frac{37}{96}e^4) + \sqrt{e^2-1}(\frac{301}{6} + \frac{673}{12}e^2)}{(e^2-1)^{\frac{7}{2}}}. \quad (6)$$

For binary capture, δE should exceed the kinetic energy $\frac{\eta M w^2}{2}$. For an MW-like galaxy with virial velocity $\sim 150\ {\rm km\,s^{-1}}$, energy loss normalized by kinetic energy equals

$$E_n \equiv \frac{\delta E}{KE} = \frac{16}{15}\eta w^5 f(e) \leq \frac{4\times10^{-15}}{15} f(e)\,, \quad (7)$$

where equality holds when the two masses are equal. This is plotted in Figure 2. From the plot we can observe that the capture condition can only be met with $e \sim 1$. Thus we can restrict our attention to near-parabolic orbits only.

At this limit, the maximum impact parameter is given by

$$b_{\max} = M[\frac{340\eta}{3\cos(1)w^9}]^{\frac{1}{7}} . \tag{8}$$

Using this, we can verify that e is indeed very close to 1. From $b_{\max}$, the capture cross section is expressed as

$$\sigma = \pi b_{\max}^2 . \tag{9}$$

Also, without considering tidal effect, a naive capture rate can be calculated as

$$R_1 = \int \frac{n(\boldsymbol{r}, \boldsymbol{v_1}) n(\boldsymbol{r}, \boldsymbol{v_2})}{2} \sigma w d\boldsymbol{r} d\boldsymbol{v_1} d\boldsymbol{v_2} , \tag{10}$$

where n is the PBH number density. From this very simple consideration, we see that the capture rate is independent of the PBH mass, as $n^2 \sim m_{\rm PBH}^{-2}$, and $\sigma \sim m_{\rm PBH}^2$ as viewed from Equation (8) and Equation (9).

4 TIDAL DISRUPTION

From Section 2, we have seen that PBH DM density peaks near the SMBH, where the tidal effect is significant. This would influence binary formation in at least two ways: on one hand the capture condition must also incorporate the tidal force, that the energy lost in GW radiation should result in a binary close enough to resist the tidal tear; on the other hand, if some formed binaries move too close to the SMBH, the tidal force might become strong enough to break the binary. It is evident that from the first effect, not the whole capture cross section is effective; from the second effect, we need to determine the directions of motion that will result in tidal disruption of formed binaries, known as the 'loss cone' (Merritt 2013), and exclude the binary population within. We will take account of these two aspects in this section.

To quantify the tidal effect, we note that it is dependent on the object's size, in this case being the binary semi-major axis. For a binary of mass M and semi-major axis a, the tidal force outweighs its gravitational attraction if the binary falls closer to the SMBH than the tidal distance (Miller et al. 2005)

$$r_t = a \sqrt[3]{\frac{M_\bullet}{M}} . \tag{11}$$

The actual disruption distance would be the larger of r_t and $r_{\rm cap}$, which we denote as r_d.

The semi-major axis is dependent on capture conditions (Cholis et al. 2016)

$$a = \frac{M}{w^2[(\frac{b_{\max}}{b})^7 - 1]} . \tag{12}$$

Thus it is evident that the actual impact parameter b within $b_{\max}$ shall be closely examined, as it results in a captured binary with different sizes, which correspond to different disruption distance r_d.

We also note that the binary size is positively related to the mass of the binary, and the same goes for the tidal disruption radius. Thus heavier PBHs tend to form wider binaries which are subject to larger disruption radii. Combined with results inferred from Section 3, we can expect lighter PBH binaries to be less affected by the tidal effect.

4.1 Effective Binary Capture

In Section 3, the capture condition does not take into account the tidal force, thus we name it a naive capture. If such a capture happens within the disruption distance to the SMBH, the binary will not form. Thus an effective binary capture must happen outside r_d. We consider $30\,M_\odot$ PBHs comprising all DM, moving isotropically at velocities calculated differently for different regions. Within the spike profile, we take $v = \sqrt{\frac{M_\bullet}{r}}$ as DM is negligible compared to the mass of the SMBH. Beyond that, DM mass cannot be neglected, and for simplicity we use the virial velocity of the galaxy $v_{\rm vir} \sim 150\,{\rm km\,s^{-1}}$. Based on Equation (10), the effective capture rate $R_{\rm eff}$ is calculated by excluding those naively captured binaries within the disruption distance:

$$\begin{aligned}
R &= \int\int \frac{n(\boldsymbol{r}, \boldsymbol{v_1}) n(\boldsymbol{r}, \boldsymbol{v_2})}{2} w d\boldsymbol{r} d\boldsymbol{v_1} d\boldsymbol{v_2} \\
&\quad \int_0^{b_{\max}(w)} 2\pi b db \Theta(r - r_d(w, b)) \\
&= \int \frac{n(\boldsymbol{r})^2}{2} 4\pi r^2 dr \int \frac{w}{(4\pi)^2} d\boldsymbol{v_1} d\boldsymbol{v_2} \\
&\quad \int_0^{b_{\max}} 2\pi b db \Theta(r - r_d) \\
&= \int \frac{n(\boldsymbol{r})^2}{2} 4\pi r^2 dr \int \frac{w}{(4\pi)^2} d\boldsymbol{v_{\rm com}} d\boldsymbol{w} \\
&\quad \int_0^{b_{\max}} 2\pi b db \Theta(r - r_d) \\
&= \int \frac{n(\boldsymbol{r})^2}{2} 4\pi r^2 dr \int \frac{2v \sin\frac{\theta_r}{2}}{4\pi} 2\pi \sin\theta_r d\theta_r \\
&\quad \int_0^{b_{\max}} 2\pi b db \Theta(r - r_d) \\
&= \frac{8\pi^2}{m^2} \int \rho(\boldsymbol{r})^2 r^2 v dr \int (\sin\frac{\theta_r}{2})^2 \cos\frac{\theta_r}{2} d\theta_r \\
&\quad \int_0^{b_{\max}} b db \Theta(r - r_d) ,
\end{aligned} \tag{13}$$

where we have included a Heaviside function $\Theta(r - r_d)$ to exclude those naively captured binaries within the

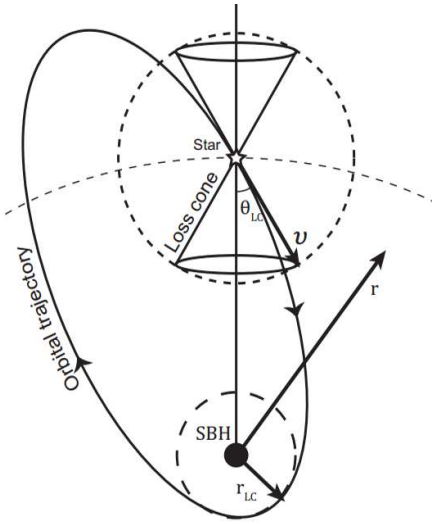

Fig. 3 Illustration of loss cone, where the binary is positioned at the 'Star' position, and SBH marks the location of the SMBH.

disruption distance, without which the integral reduces to Equation (10). In the second line we apply isotropy in the velocity space, whose independence between two populations enables us to change to center-of-mass (C.O.M.) and relative velocity spaces in line three, and by integrating out irrelevant variables in the second integral we keep the polar angle θ_r between two velocities.

Note that the mass at the front does not signify dependence, as it also appears in $b_{\max}$ as in Equation (8); nor is the radial integral self contained, as r appears in the last integral as well. The only relation is that the effective capture rate scales with density squared.

As stated before, we will use the spike profile to account for the region within 0.2 pc, the segregated profile out to 200 pc and NFW outwards. Results are summarized in Table 1, with the naive capture rate also listed for comparison.

4.2 Loss Zone and Loss Cone

Upon effective binary formation, some fraction moving too close to the SMBH would gradually enter the disruption distance before merging itself. This range of directions was given the name loss cone (Merritt 2013). For a specific binary with semi-major axis a, there is a critical angular momentum $l_{\rm crit}$ such that the binary would graze the sphere of tidal disruption.

$$l_{\rm crit} = r_d\sqrt{v_{\rm com}^2 - \frac{2M_\bullet}{r} + \frac{2M_\bullet}{r_d}}\,. \tag{14}$$

The corresponding directions of motion form the boundary of the loss cone, illustrated in Figure 3 directly adopted from Merritt (2013).

Thus to account for this effect, we need to exclude those effectively captured binaries moving within the loss

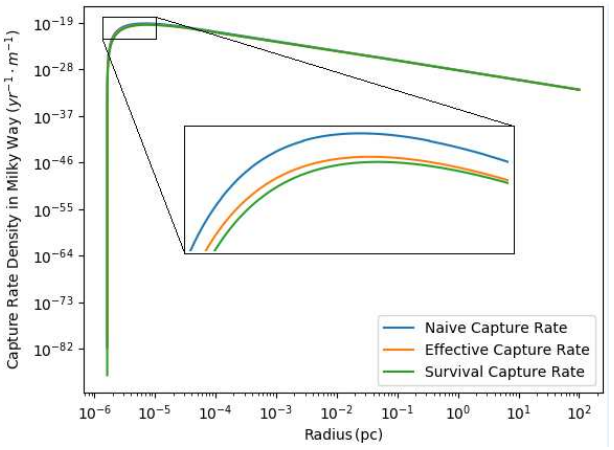

Fig. 4 Capture rate density in MW, with window showing the peak region, where the three curves differ the most.

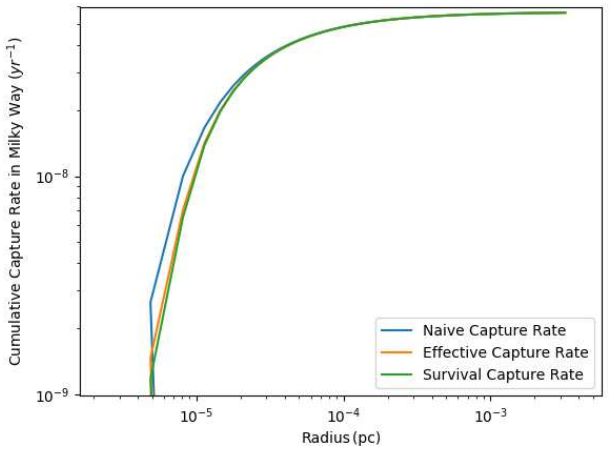

Fig. 5 Cumulative capture rate in the MW.

cone. In the literature, the loss cone has been assumed to be small (Merritt 2013). We found, however, by comparing the critical angular momentum (Eq. (14)) with $v \times r$ for a binary with its corresponding r_d, there is a radial distance within which the critical angular momentum becomes larger than $v \times r$, which means the binary will always enter the disruption distance whichever direction it moves; or equivalently, the loss cone covers the whole solid angle. We name this radial distance the 'loss zone' distance, for a specific binary configuration.

$$r_z = r_d\frac{\sqrt{1+\frac{8M_\bullet}{v_{\rm com}^2 r_d}}-1}{2}\,. \tag{15}$$

Thus the loss cone angle should be computed as

$$\theta_l = \begin{cases} \arcsin(\frac{l_{\rm crit}}{v_{\rm com}r}) & r > r_z, r > r_d \\ \frac{\pi}{2} & \text{else} \end{cases}\,. \tag{16}$$

To account for this effect, Equation (13) should be further modified, where the integration of binary C.O.M.

directions of motion should be screened as well.

$$\begin{aligned} R &= \int \frac{n(\boldsymbol{r})^2}{2} 4\pi r^2 dr \int \frac{w}{4\pi} d\boldsymbol{w} \int_0^{b_{\max}} 2\pi b db \\ &\quad \int_{\theta_l}^{\pi-\theta_l} \frac{1}{4\pi} d\boldsymbol{v}_{\mathbf{com}} \\ &= \frac{8\pi^2\sqrt{M_\bullet}}{m^2} \int \rho^2 r^{1.5} dr \int \sin\frac{\theta_r}{2}^2 \cos\frac{\theta_r}{2} d\theta_r \\ &\quad \int_0^{b_{\max}} b db \cos\theta_l \,. \end{aligned} \tag{17}$$

The binary capture rates for different regions are calculated and added to Table 1 as well.

5 RESULTS AND DISCUSSION

We list and compare three binary formation rates with more physics coming into play, and also look at different regions of interest where the analytic profiles differ.

It is immediately evident that the spike region dominates binary formation, while cumulatively the outskirt NFW region contributes more than the segregation region. We could also observe that the tidal force eliminates $\sim$ 30% of naively captured binaries in the spike, and the majority of the rest survive the following evolution without entering the loss cone. This effect dies down as we move away from the galactic center, and overall speaking the tidal effect does not influence binary formation rate noticeably by orders of magnitude.

To further illustrate the spatial details of binary formation, we plotted the capture rate density and cumulative capture rate for the three different methods in Figures 4 and 5 below.

From the plots we see that the two rates taking into account the tidal effect do not differ from the naive binary capture rate noticeably, thus the SMBH's tidal disruption plays no significant role in binary formation. To find out the reason, we notice that the maximum impact parameter $b_{\max}$ given by Equation (8) is inversely proportional to the magnitude of relative velocity by $w^{-\frac{9}{7}}$. Thus in the innermost region where the SMBH mass dominates the gravitational potential, the maximum impact parameter shrinks closer to the center, resulting in harder binaries. We also notice that the semi-major axis of the captured binary, expressed by Equation (12), is also inversely proportional to the relative velocity by w^{-2}. To look at the dependence on the other factor of $(\frac{b_{\max}}{b})^7 - 1$, we simulated a million binary formation events at two positions of interest to observe the distribution of binary sizes, which is depicted in Figure 6. When doing so, we assumed the same isotropy in relative velocity, i.e., $p(\theta_{\rm rel}) = \frac{1}{4\pi}$ and $w = 2v(r)\sin\frac{\theta_{\rm rel}}{2}$, where $v(r)$ is the velocity of PBHs being $\sqrt{\frac{M_\bullet}{r}}$ as in Section 4.1. For the probability distribution of impact parameter b, we assumed a uniform probability within the total capture cross section: $p(b) = \frac{2\pi b}{\sigma} = \frac{2\pi b}{\pi b_{\max}^2}$.

From the plot, we can confirm that closer to the galactic center, the overall binary sizes do shrink. The reduction in capture cross section and increase in PBH velocity results in the compactness of captured binaries. On the other hand, the reduction in capture cross section is compensated by the increase in the density of the PBHs near the galactic center, so the capture rate is dominated by the spike region. Thus we recover the results in Table 1, that the innermost region dominates binary capture rate, and the tidal effect is not prominent in affecting binary formation.

After the binary formation in a single MW-like galaxy has been identified, it can be convolved with the halo mass function to compute the binary formation rate per comoving volume and compared with LIGO's estimation of 0.5–12 $\mathrm{Gpc}^{-3}\,\mathrm{yr}^{-1}$, which was later raised to 9.7–101 $\mathrm{Gpc}^{-3}\,\mathrm{yr}^{-1}$ with all ten binary BH detections considered (Abbott et al. 2016; Abbott et al. 2019). During this work, there has been a similar study coming out that used the naive capture rate at the spike region and three SMBH mass functions to calculate the total rate density in halos hosting an SMBH (Nishikawa et al. 2017). The result is adopted here as Figure 7. Note that the shaded region showing LIGO's event rate estimation should be shifted upward to reflect the most updated value. Since we have confirmed that the tidal effect does not change the binary formation rate by orders of magnitude, the conclusion drawn from this figure is unaltered. From the plot, even the most optimistic estimation can only reach the lower bound of LIGO's estimation near $\gamma = 1$. Thus, it is not very likely that halos with SMBHs alone gave rise to LIGO's detection.

Besides this sub-group, we also need to incorporate the contribution from halos without SMBHs, especially from those small halos whose signals actually dominate (Nishikawa et al. 2017; Bird et al. 2016). Thus we refer to Bird et al. (2016), which calculated the total merger rate for all halos implementing the simple NFW profile. By including halos as small as $400\,M_\odot$, the total merger rate is around 2 $\mathrm{Gpc}^{-3}\,\mathrm{yr}^{-1}$. With these two results combined, we see that the total rate is still barely comparable to the lower limit of LIGO's estimation. Unless the actual physical situation deviates from the modeling noticeably, it is not likely that PBH DM with a monochromatic mass of $30\,M_\odot$ alone explains the GW signal.

Even more importantly, a lensing event, MACS J1149 LS1, was later observed, where a background star at z=1.49 experienced a transient magnification of several thousand times and qualifies as a caustic crossing event (Kelly et al. 2018). A caustic curve, or caustic, is the line joining the locations of the largest magnification on the

Table 1 Capture Rate at Different Regions

Distance	$r_{\rm cap}$ – 0.2 pc	0.2 – 200 pc	200 – Mpc
Profile	Spike	Segregated	NFW
Naive capture/halo	$5.60 \times 10^{-8}\,{\rm yr}^{-1}$	$6.24 \times 10^{-11}\,{\rm yr}^{-1}$	$6.29 \times 10^{-9}\,{\rm yr}^{-1}$
Effective capture/halo	$3.93 \times 10^{-8}\,{\rm yr}^{-1}$	$5.73 \times 10^{-11}\,{\rm yr}^{-1}$	$5.82 \times 10^{-9}\,{\rm yr}^{-1}$
Outside Loss Cone/halo	$3.69 \times 10^{-8}\,{\rm yr}^{-1}$	$5.64 \times 10^{-11}\,{\rm yr}^{-1}$	$5.74 \times 10^{-9}\,{\rm yr}^{-1}$

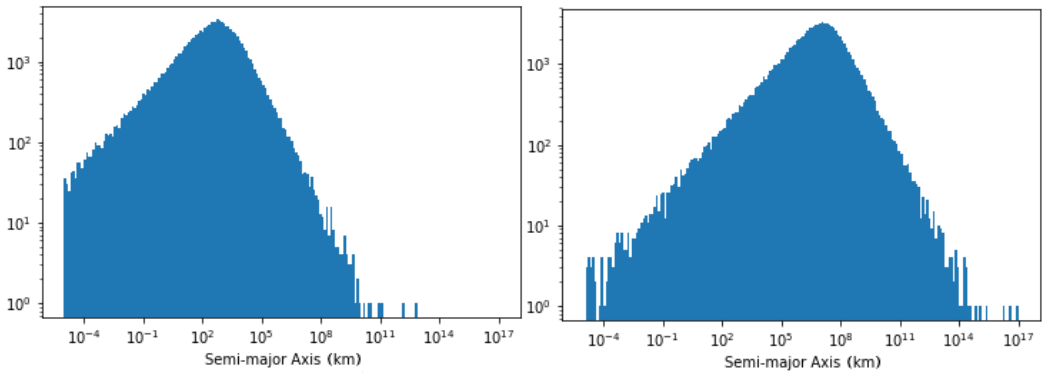

Fig. 6 Counts of simulated binary size for one million runs. *Left*: at 10^{-5} pc. *Right*: at 0.2 pc where the validity region of the spike profile was assumed to terminate.

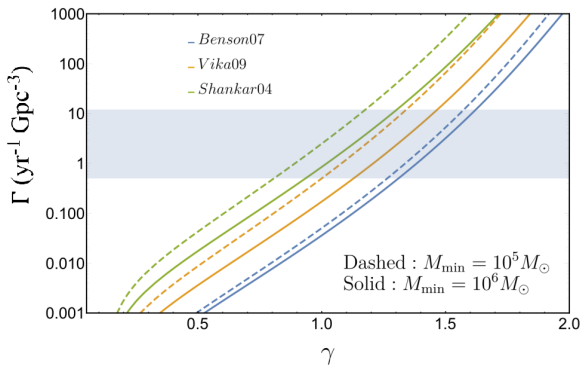

Fig. 7 Binary formation rate density with three different halo mass functions, with *solid* and *dotted lines* signifying different minimum halo masses, plotted against the power index of the initial PBH distribution, where for an NFW profile we look at $\gamma = 1$. The *shaded region* represents the rate 0.5–12 Gpc^{-3} yr^{-1} estimated by LIGO (Abbott et al. 2016).

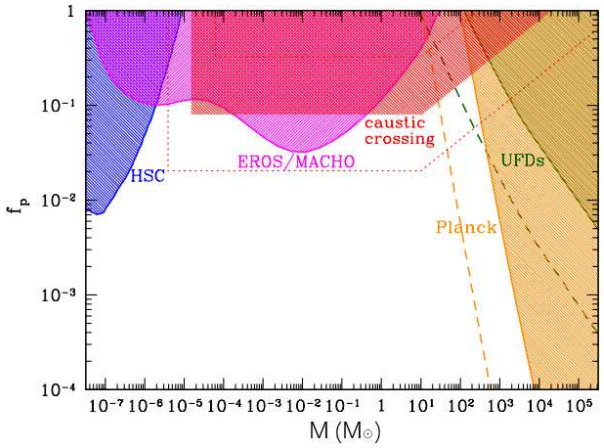

Fig. 8 Constraints on the mass (M) and fraction of compact DM. Shaded regions indicate the excluded range by caustic crossing of MACS J1149 LS1, M31 microlensing by Subaru/Hyper Suprime-Cam (HSC) (Niikura et al. 2017), EROS/MACHO microlensing (Alcock et al. 2000; Tisserand et al. 2007), ultra-faint dwarf galaxies (UFD) (Brandt 2016) and Planck cosmic microwave background observations (Planck) (Ali-Haïmoud & Kamionkowski 2017). For caustic crossing, *dotted lines* demonstrate the effect with different assumed transverse velocities, being twice and half of the fiducial value. For UFDs and Planck, *dotted lines* signify more stringent limits compared with the conservative ones in *solid lines*.

source plane. Such geometrical property is influenced by the distribution of lenses in the foreground. A follow-up study demonstrated that the existence of abundant massive compact DM such as a $30\,M_\odot$ PBH would break the condition for the formation of the caustic. Monochromatic PBH DM of $30\,M_\odot$ is thus further constrained on the mass-fraction plane as illustrated in Figure 8 (Oguri et al. 2018).

We can see that the whole mass window of PBH on the order of $10 \sim 100\,M_\odot$ has been constrained well to $\sim 10\%$ of total DM. As we have affirmed that the binary formation rate is proportional to the density squared as in Equations (10, 13, 17), the new constraint from the caustic crossing event reduces the calculated binary formation rate in Section 5 by two orders of magnitude. Thus it not only constrains monochromatic PBH to constitute a major

fraction of DM, but implies that it is very unlikely that LIGO's detection signals originate from $30\,M_\odot$ PBH DM.

However, it was later argued that a binary PBH could form via another channel in the early days of the universe, roughly at matter-radiation equality, and that two PBHs forming close enough would have enough gravitational attraction to decouple from cosmic expansion (Sasaki et al. 2016; Hayasaki et al. 2016; Ali-Haïmoud et al. 2017). The corresponding merger rate was found to coincide with LIGO's estimation if PBHs only constitute $\sim$ 1% of DM. This is consistent with the current constraints on PBH DM mentioned before in Figure 8. Or rather, it further constrains PBH DM based on LIGO's detections. Another study took a step forward in computing the merger rate from early formed PBH binaries with two types of typical extended mass functions, namely power-law and log-normal, and found agreement that LIGO constrains $M_\odot \sim 100\,M_\odot$ PBHs to constitute $10^{-3} \sim 10^{-2}$ of DM (Chen & Huang 2018). Thus we see that LIGO might indeed have detected mergers of binary PBHs formed in the early universe, yet they only account for around one percent of total DM at most.

From Figure 8 we see that PBH DM in the mass range across $10^{-7} \sim 10^{6}\,M_\odot$ has been well constrained below $\sim$ 1 percent. Constraints are also present across lower mass ranges, yet there still remains a major window around $10^{-15} \sim 10^{-11}\,M_\odot$ due to the debate over the constraints imposed by the capture of NSs (Capela et al. 2013), which relies on the premise that DM exists in the cores of globular clusters (Sasaki et al. 2018). Thus it is still promising that PBHs constitute a major fraction of DM, but not of the masses typical of LIGO detections.

6 CONCLUSIONS

LIGO's frequently detected binary BH mergers of $\sim 30\,M_\odot$ can be fully attributed to PBH binaries formed in the early universe. The event rate constrains PBHs at $\sim 30\,M_\odot$ to comprise DM below one percent. PBH DM could also form binaries via close-encounters in the late universe, which is dominated by the central region of the halo where DM density is supposed to form a spike. At such vicinity of the SMBH at the galactic center, whose tidal effect is expected to be strong, we have shown that it has no significant impact on binary formation. When doing so, we have discovered an essential notion called 'loss zone' that complements the usage of 'loss cone' in evaluating the tidal effect on the fate of the object of interest. However, this late binary formation channel corresponds to a much lower event rate, approximately four orders smaller. Yet the loss zone notion is not restricted to this scenario only, and should apply wherever loss cone is applied.

Altogether, LIGO might have detected binary mergers of PBH DM that formed in the early universe. Such detection also constrains the fraction of PBH around 30 solar masses in DM below one percent. Thus DM retains its mystery, and people should keep searching for alternative PBH windows and other candidate DM.

Acknowledgements We would like to thank Dr. Ilias Cholis, Mr. Qinan Wang, Mr. Hong Tsun Wong, Mr. Jianju Tang and Mr. Renjiu Hu for the fruitful discussions in carrying out this research work.

References

Abbott, B. P., et al. 2017a, ApJ, 851, L35
Abbott, B. P., et al. 2017b, Phys. Rev. Lett., 119, 141101
Abbott, B. P., et al. 2019, Physical Review X, 9, 031040
Abbott, B. P., et al. 2016, Physical Review X, 6, 041015
Abbott, B. P., Abbott, R., Abbott, T. D., et al. 2016a, Phys. Rev. Lett., 116, 241103
Abbott, B. P., Abbott, R., Abbott, T. D., et al. 2016b, Phys. Rev. Lett., 116, 061102
Abbott, B. P., Abbott, R., Abbott, T. D., et al. 2017, Phys. Rev. Lett., 118, 221101
Alcock, C., Allsman, R. A., Alves, D. R., et al. 2000, ApJ, 542, 281
Ali-Haïmoud, Y., & Kamionkowski, M. 2017, Phys. Rev. D, 95, 043534
Ali-Haïmoud, Y., Kovetz, E. D., & Kamionkowski, M. 2017, Phys. Rev. D, 96, 123523
Bird, S., Cholis, I., Muñoz, J. B., et al. 2016, Phys. Rev. Lett., 116, 201301
Brandt, T. D. 2016, ApJ, 824, L31
Capela, F., Pshirkov, M., & Tinyakov, P. 2013, Phys. Rev. D, 87, 123524
Carr, B., Kühnel, F., & Sandstad, M. 2016, Phys. Rev. D, 94, 083504
Chapline, G. F. 1975, Nature, 253, 251
Chen, Z.-C., & Huang, Q.-G. 2018, ApJ, 864, 61
Cholis, I., Kovetz, E. D., Ali-Haïmoud, Y., et al. 2016, Physical Review D, 94, 084013
Clesse, S., & García-Bellido, J. 2015, Phys. Rev. D, 92, 023524
Corbelli, E., & Salucci, P. 2000, MNRAS, 311, 441
Courteau, S., & Dutton, A. A. 2015, ApJ, 801, L20
Gondolo, P., & Silk, J. 1999, Physical Review Letters, 83, 1719
Hayasaki, K., Takahashi, K., Sendouda, Y., et al. 2016, PASJ, 68, 66
Jungman, G., Kamionkowski, M., & Griest, K. 1996, Phys. Rep., 267, 195
Kelly, P. L., Diego, J. M., Rodney, S., et al. 2018, Nature Astronomy, 2, 334
Lee, M. H. 1993, ApJ, 418, 147
Merritt, D. 2013, Classical and Quantum Gravity, 30, 244005
Merritt, D., Alexander, T., Mikkola, S., et al. 2011, Physical Review D, 84, 044024

Merritt, D., Graham, A. W., Moore, B., et al. 2006, ApJ, 132, 2685
Miller, M. C., Freitag, M., Hamilton, D. P., et al. 2005, ApJ, 631, L117
Navarro, J. F., Frenk, C. S., & White, S. D. M. 1997, ApJ, 490, 493
Niikura, H., Takada, M., Yasuda, N., et al. 2017, arXiv e-prints, arXiv:1701.02151
Nishikawa, H., Kovetz, E. D., Kamionkowski, M., et al. 2017, arXiv e-prints, arXiv:1708.08449
Oguri, M., Diego, J. M., Kaiser, N., et al. 2018, Phys. Rev. D, 97, 023518
O'Leary, R. M., Kocsis, B., & Loeb, A. 2009, MNRAS, 395, 2127
Preskill, J., Wise, M. B., & Wilczek, F. 1983, Physics Letters B, 120, 127
Quinlan, G. D., & Shapiro, S. L. 1989, ApJ, 343, 725
Sasaki, M., Suyama, T., Tanaka, T., et al. 2016, Phys. Rev. Lett., 117, 061101
Sasaki, M., Suyama, T., Tanaka, T., et al. 2018, Classical and Quantum Gravity, 35, 063001
Tisserand, P., Le Guillou, L., Afonso, C., et al. 2007, A&A, 469, 387
Turner, M. 1977, ApJ, 216, 610